Broadband tunable optical amplification based on modulation instability characteristic of high-birefringence photonic crystal fibers*

Wang He-Lin(王河林)[a)†], Yang Ai-Jun(杨爱军)[a)], and Leng Yu-Xin(冷雨欣)[b)]

[a)] College of Science, Zhejiang University of Technology, Hangzhou 310023, China

[b)] State Key Laboratory of High Field Laser Physics, Shanghai Institute of Optics and Fine Mechanics, Chinese Academy of Sciences, Shanghai 201800, China

(Received 17 October 2012; revised manuscript received 8 January 2013)

A novel high-birefringence photonic crystal fiber (HB-PCF) with two zero-dispersion wavelengths (ZDWs) is designed, and an extraordinarily high modal birefringence of 1.56×10^{-2} is obtained at pump wavelength $\lambda_p = 1850$ nm. With the designed HB-PCF, the effect of the pump parameters on the modulation instability (MI) in the anomalous dispersion region close to the second ZDWs of the HB-PCF is comprehensively studied in this work. A broadband and tunable optical amplification is achieved by controlling the pump power and the pump wavelength based on the combined operation of Raman effect and cross phase modulation. By optimizing the pump parameters, the amplification bandwidth along the fiber slow axis reaches 152 nm for the pump power $P_p = 280$ W and the pump wavelength λ_p=1675 nm, while the gain bandwidth along the fiber fast axis is 165 nm for the pump power $P_p = 600$ W and the pump wavelength $\lambda_p = 1818$ nm.

Keywords: modulation instability, broadband amplification, high-birefringence fiber

PACS: 42.65.Sf, 42.65.Wi **DOI:** 10.1088/1674-1056/22/7/074208

1. Introduction

Modulation instability (MI) is a special four-wave mixing (FWM) process in the fiber,[1–3] which has attracted much attention for supercontinuum (SC) generation and broadband amplification in some experimental investigations.[4–6] Due to an interplay between the nonlinear and the dispersive effects, MI usually appears in the anomalous group velocity dispersion (GVD) regime.[7] However, MI may also occur in the normal GVD regime in some special cases, such as in the presence of higher even-order linear dispersions[8] and the co-propagation of two or more optical fields in an optical fiber.[9] Many researchers have studied MI in optical fibers and found that its practical application is extensive. For example, the MI gain may be exploited as a relatively broadband and tunable gain mechanism in highly nonlinear fiber-based frequency converters[10,11] and oscillators.[12,13] But most works mainly discussed the effect of the cross phase modulation (XPM) on the MI,[14] and disregarded the combination effect of XPM and Raman scattering (RS). Moreover, the studies were usually limited to low birefringence or no birefringence optical fibers, and paid little attention to the modulation stability gain characteristic in the high-birefringence (HB) fiber, especially the high-birefringence photonic crystal fiber (HB-PCF). Therefore, as a promising technique for providing broadband amplification, the MI gain property including XPM and RS is a worthwhile research topic in the HB-PCF.

In this work, we first design a novel high-birefringence photonic crystal fiber with two zero-dispersion wavelengths (ZDWs), and study an interesting situation when the pump wavelength is close to the second ZDW of the fiber in the anomalous dispersion region. With a more precise coupled nonlinear Schrödinger equation (CNSE), the effects of high-order dispersion, pump wavelength, and power on the MI gain are analyzed, and the combined contribution of XPM and RS to the MI gain bandwidth is discussed.

2. Modulation instability gain model for HB-PCF

In the HB-PCF, the dispersion characteristics of the fiber slow and fast axes are significantly different. So assuming that the dispersion profiles are the same, which is usually used for the low birefringence fibers, may not be adequate in this case. Therefore, a more precise model becomes necessary for the analysis of such an HB fiber. In this work, by considering the polarization coupling effect and the group delay, a model with coupled nonlinear Schrödinger equations is adopted, and many nonlinear physical processes, such as self-phase modulation (SPM), FWM, self-steepening (SS), XPM, and RS,[15–17] are considered. They are defined in terms of linear polarization components

$$\frac{\partial A_j}{\partial z} + (-1)^{j+1}\delta\beta_1\frac{\partial A_j}{\partial T} + \frac{\alpha}{2}A_j + \sum_{n\geq 2}\frac{\mathrm{i}^{n-1}\beta_{nj}}{n!}\frac{\partial^n A_j}{\partial T^n}$$
$$= \mathrm{i}\gamma_j\left(1+\mathrm{i}\tau_j\frac{\partial}{\partial T}\right)\left\{(1-f_R)\left[A_j|A_j|^2+\frac{2}{3}A_j|A_{3-j}|^2\right.\right.$$

*Project supported by the National Natural Science Foundation of China (Grant No. 11226148), the Scientific Research Foundation of Zhejiang Province, China (Grant No. LY12F05006), and the Education Department Foundation of Zhejiang Province, China (Grant No. Y201121906).

†Corresponding author. E-mail: whl982032@163.com

© 2013 Chinese Physical Society and IOP Publishing Ltd

$$+\frac{1}{3}A_j^* A_{3-j}^2 \exp\left((-1)^j 2\mathrm{i}\Delta\beta z\right)\Big]$$
$$+f_{\mathrm{R}}\Big[A_j\int_{-\infty}^{T} f_1(T-s)\left|A_j(s)\right|^2 \mathrm{d}s$$
$$+A_j\int_{-\infty}^{T} f_2(T-s)\left|A_{3-j}(s)\right|^2 \mathrm{d}s$$
$$+A_{3-j}\int_{-\infty}^{T} f_3(T-s)(A_j(s)A_{3-j}^*(s)$$
$$+A_j^*(s)A_{3-j}(s)\exp\left((-1)^j 2\mathrm{i}\Delta\beta z\right))\mathrm{d}s\Big]\Big\}, \quad (1)$$

where $A_{j=1(x),2(y)}$ are the normalized amplitudes corresponding to the fiber slow (x) and fast (y) axes, respectively, α is the loss coefficient of the fiber, z is the longitudinal traveling distance, $T = t - z(\beta_{11}+\beta_{12})/2$ is the normalized time in a reference frame moving at the group velocity, and $\beta_{nj} = \partial^n \beta_j/\partial\omega^n$ is the n-th order dispersion coefficient for the propagation constant β_j. The $\delta\beta_1 = (1/V_{\mathrm{g1}} - 1/V_{\mathrm{g2}}) = (\beta_{11}-\beta_{12})/2$ is the group velocity mismatch between the two polarization modes, V_{g1} and V_{g2} are their group velocities, $\Delta\beta = \beta_{01} - \beta_{02} = 2\pi/L_{\mathrm{B}} = (2\pi/\lambda_{\mathrm{p}})\Delta n$, β_{01} and β_{02} are the mode propagation constants along the fiber slow and fast axes, respectively, L_{B} is the beat length, and $\Delta n = n_1(\lambda_{\mathrm{p}}) - n_2(\lambda_{\mathrm{p}})$ is the refractive index difference between the fiber slow and fast axes. The $\tau_j = 1/\omega_{\mathrm{p}}$, ω_{p} is the central frequency of the pump light. The $\gamma_j = n_2\omega_{\mathrm{p}}/cA_{\mathrm{eff},j}(\omega)$ is the nonlinear coefficient, $n_{\mathrm{eff}}(\omega)$ is the effective refractive index of the fiber, $A_{\mathrm{eff},j}(\omega)$ is the effective cross sectional area of the guided mode, and $n_2 = 2.6\times10^{-20}$ m$^2\cdot$W^{-1} is the nonlinear refractive index coefficient of silica glass. The $f_{\mathrm{R}} = 0.18$ is the fraction of the Raman contribution to the Kerr effect, $f_1(t)$, $f_2(t)$, and $f_3(t)$ can be written as[18–20]

$$\begin{aligned} f_1(t) &= [R_{\mathrm{a}}(t)+R_{\mathrm{b}}(t)]/2, \\ f_2(t) &= R_{\mathrm{a}}(t)/2, \quad f_3(t) = R_{\mathrm{b}}(t)/4, \end{aligned} \quad (2)$$

with

$$\begin{cases} R_{\mathrm{a}}(t) = f_{\mathrm{a}}h_{\mathrm{a}}(t), \\ R_{\mathrm{b}}(t) = f_{\mathrm{b}}h_{\mathrm{b}}(t) + f_{\mathrm{c}}h_{\mathrm{a}}(t), \end{cases}$$
$$\begin{cases} h_{\mathrm{a}}(t) = \left[(t_1^2+t_2^2)/t_1t_2^2\right]\exp(-t/t_2)\sin(t/t_1), \\ h_{\mathrm{b}}(t) = \left[(2t_{\mathrm{b}}-t)/t_{\mathrm{b}}^2\right]\exp(-t/t_{\mathrm{b}}), \end{cases}$$

where $t_1 = 12.2$ fs, $t_2 = 32$ fs, $t_{\mathrm{b}} = 96$ fs, $f_{\mathrm{a}} = 0.75$, $f_{\mathrm{b}} = 0.21$, $f_{\mathrm{c}} = 0.04$, $R_{\mathrm{a}}(t)$, and $R_{\mathrm{b}}(t)$ are the isotropic and anisotropic parts of the Raman response, respectively, and $f_1(t)$ and $f_2(t)$ represent the parallel and orthogonal components of the Raman response, respectively. In the above CNSE, the second line accounts for SPM, XPM, and degenerated FWM, the third and the fourth lines account for the Raman effect. According to Ref. [18], the term which is responsible for the degenerate FWM between orthogonal components can be ignored when the fiber length is much longer than the beat length.

As far as the HB-PCF is concerned, the continuous wave (CW) and the quasi-continuous wave are unstable whenever their polarizations lie between the fast and the slow axes of the fiber, whereas a beam which is exactly aligned along one of the two birefringence axes is modulation stability. By restricting our analysis to under the undepleted-pump approximation, the modulation instability in the CNSE is revealed by a linear stability analysis of its solution

$$\begin{aligned} A_j(z) &= \left(\sqrt{P_j}\right)\exp\left[\mathrm{i}\gamma_j\left(P_j+2P_{3-j}/3\right)z\right], \\ &\quad (j=1,2), \end{aligned} \quad (3)$$

where $P_{j=1,2}$ are the pump powers along the fiber slow and fast axes, respectively, $P_1 = P_0\cos^2\theta$, $P_2 = P_0\sin^2\theta$, P_0 is the total power of the pump light, and θ is the polarization angle of the pump light with respect to the fiber slow axis. To investigate the effect of small perturbations on the steady solution (3), the first-order perturbations $u_{j(j=1,2)}$ are introduced as

$$\begin{aligned} A_j(z,t) &= \left(\sqrt{P_j}+u_j\right)\exp\left[\mathrm{i}\gamma_j\left(P_j+2P_{3-j}/3\right)z\right], \\ &\quad (j=1,2), \end{aligned} \quad (4)$$

where $u_1(z,t) = u_{\mathrm{s}}(z)\exp(\mathrm{i}\Omega t) + u_{\mathrm{as}}(z)\exp(-\mathrm{i}\Omega t)$, $u_2(z,t) = \upsilon_{\mathrm{s}}(z)\exp(\mathrm{i}\Omega t) + \upsilon_{\mathrm{as}}(z)\exp(-\mathrm{i}\Omega t)$, $u_{\mathrm{s}}(z)$ and $u_{\mathrm{as}}(z)$ are the small signal amplitudes of the Stokes and the anti-Stokes waves along the fiber slow axis, while $\upsilon_{\mathrm{s}}(z)$ and $\upsilon_{\mathrm{as}}(z)$ are the small signal amplitudes of the Stokes and the anti-Stokes waves along the fiber fast axis at frequency shifts $\pm\Omega$, respectively, and $\Omega = \omega_{\mathrm{p}} - \omega_{\mathrm{s}} = \omega_{\mathrm{as}} - \omega_{\mathrm{p}}$ ($\Omega > 0$). After inserting Eq. (4) into Eq. (1), four coupled linear ordinary differential equations are obtained by picking out the anti-Stokes term and the complex conjugate of the Stokes term and making them linearized. They can be written as

$$\begin{aligned} \frac{\mathrm{d}}{\mathrm{d}z}\begin{pmatrix} u_{\mathrm{as}}(z) \\ u_{\mathrm{s}}^*(z) \\ \upsilon_{\mathrm{as}}(z) \\ \upsilon_{\mathrm{s}}^*(z) \end{pmatrix} &= \mathrm{i}\begin{pmatrix} M_{11} & M_{12} & M_{13} & M_{14} \\ M_{21} & M_{22} & M_{23} & M_{24} \\ M_{31} & M_{32} & M_{33} & M_{34} \\ M_{41} & M_{42} & M_{43} & M_{44} \end{pmatrix}\begin{pmatrix} u_{\mathrm{as}}(z) \\ u_{\mathrm{s}}^*(z) \\ \upsilon_{\mathrm{as}}(z) \\ \upsilon_{\mathrm{s}}^*(z) \end{pmatrix} \\ &= \mathrm{i}\boldsymbol{M}\begin{pmatrix} u_{\mathrm{as}}(z) \\ u_{\mathrm{s}}^*(z) \\ \upsilon_{\mathrm{as}}(z) \\ \upsilon_{\mathrm{s}}^*(z) \end{pmatrix}, \end{aligned} \quad (5)$$

where $\boldsymbol{M}$ designates the stability matrix of the system. Suppose that $u_{\mathrm{as}}(z)$, $u_{\mathrm{s}}^*(z)$, $\upsilon_{\mathrm{as}}(z)$, and $\upsilon_{\mathrm{s}}^*(z) \propto \exp(\pm\mathrm{i}\zeta z)$ is a solution of Eq. (5), the modulation instability occurs when ζ possesses a nonzero imaginary part. The perturbation parameter ζ depends on pump wavelength, pump power, and fiber parameters, and is determined by the eigenvalues of matrix $\boldsymbol{M}$. With parameter ζ, the MI gain coefficient is usually defined as

$$G(\Omega) = 2\left|\mathrm{Im}\left(\zeta\right)\right|. \quad (6)$$

The modulation instability occurs at the detuning frequency Ω, where the Stokes or anti-Stokes wave undergoes an exponential growth.

3. HB-PCF design and characteristic

For conveniently studying the MI gain properties of the HB-PCF, we first design a novel HB-PCF (see Fig. 1) with the finite-difference frequency-domain techniques.[21] The HB-PCF is made up of circular and elliptical air holes. The two big circular air holes have diameter $d_1 = 2.26$ μm, whereas the long and the short semi-axes of the small elliptical air holes are 1.0 μm and 0.25 μm, respectively, and the pitch is $\Lambda = 2$ μm. Figure 1 shows the profiles of the x- and y-polarization fundamental modes and the field vector. The asymmetrical structure of the HB-PCF results in the high birefringence characteristics. The effective refractive index variations of the polarization mode with the wavelength along the HB-PCF x- and y-axes are shown in Fig. 2(a). It can be seen that the birefringence index of the designed HB-PCF gradually increases with the increase of the pump wavelength, and it reaches 1.5607×10^{-2} at pump wavelength 1850 nm. Besides the birefringence, the polarization mode areas and the nonlinear coefficients along the fiber x- and y-axes are different. Figure 2(b) shows that the effective polarization mode area of the HB-PCF gradually increases with the increase of the pump wavelength, while its nonlinear coefficient gradually decreases.

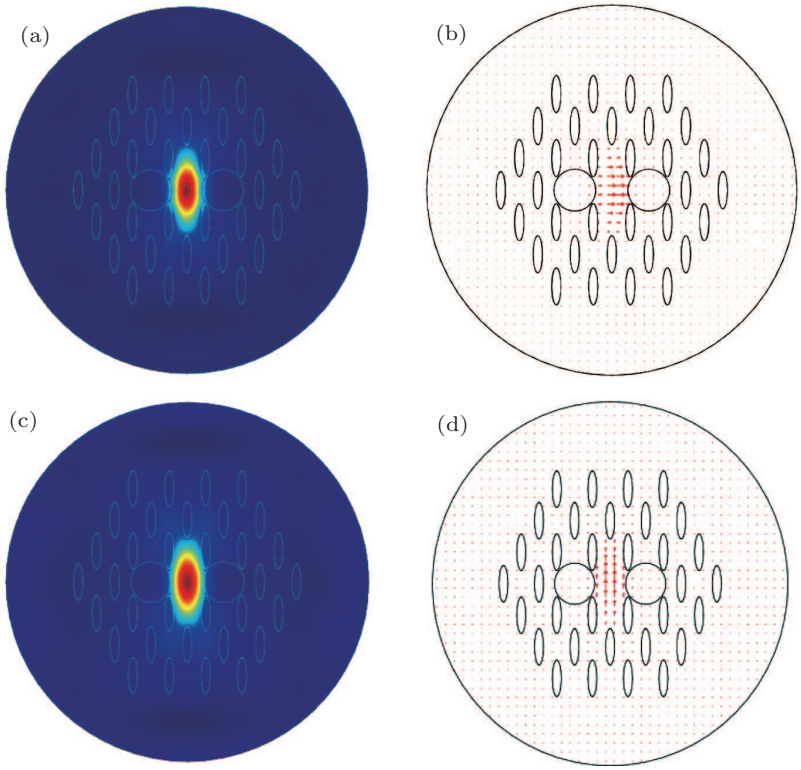


Fig. 1. (color online) Mode profiles and field vectors of HB-PCF: (a) E_x field mode profile, (b) E_x field vector, (c) E_y field mode profile, (d) E_y field vector.

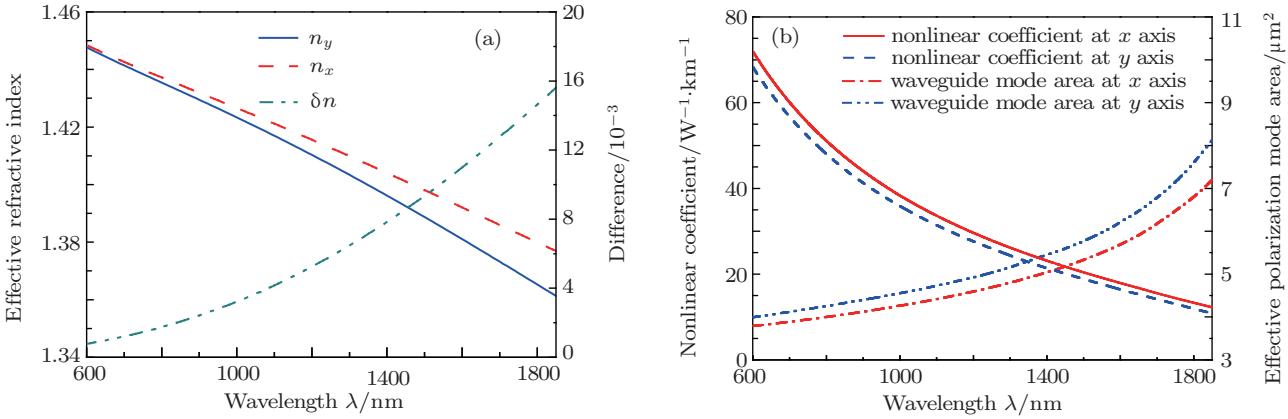


Fig. 2. (color online) (a) Effective refractive indexes along the fiber slow and fast axes and their difference. (b) Effective polarization mode areas and the nonlinear coefficients along the fiber slow and fast axes.

Since we study the broadband gain characteristics of the HB-PCF in this article, the fiber parameters (mainly including the fiber nonlinear coefficient and the dispersion, see Eq. (1)) play the most important role in affecting the broadband MI gain. Figure 3(a) gives the total dispersion characteristic of the designed HB-PCF. It is easy to see that the designed HB-PCF has two ZDWs, the two ZDWs are 791 nm and 865 nm in the visible region, while they are 1826 nm and 1683 nm in the infrared region. In the visible range, the fourth and the higher order dispersion coefficients of the HB-PCF are almost equal to 0, so the pump wavelength is chosen in the infrared region and close to their second ZDWs (1826 nm and 1683 nm) in this study. The group delay (GD) is also given in Fig. 3(b) for the fiber fast and slow axes, which shows a larger difference between the two fiber axes.

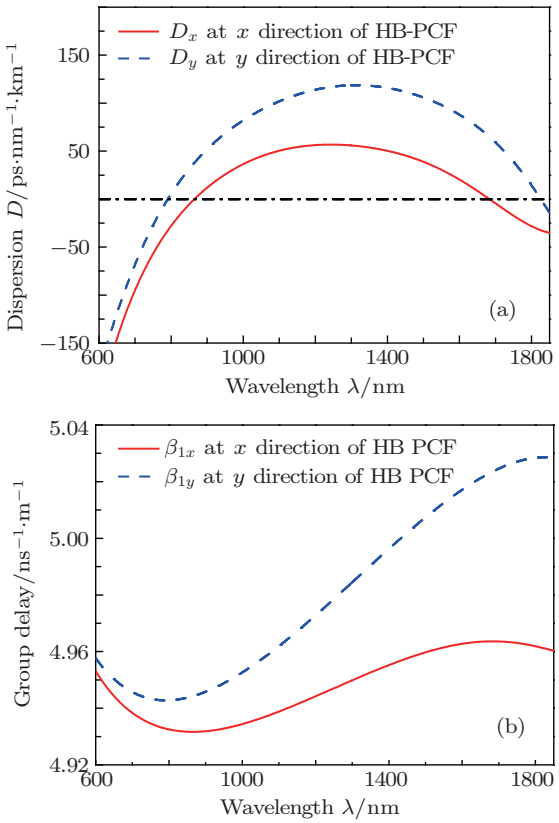


Fig. 3. (color online) (a) Total dispersion characteristic and (b) group delay versus wavelength for the fiber fast and slow axes.

4. Numerical results of broadband gain

Based on the designed HB-PCF with two ZDWs, the influences of the pump and the fiber parameters on the MI gain are studied. The pump parameters mainly include the pump power and the pump wavelength, while the fiber parameters refer to the fiber dispersion, the nonlinear coefficient, and the group delay. Figure 4 shows the MI gain versus the frequency shift at six different pump wavelengths. For the fiber slow axis, the six different pump wavelengths are chosen to be close to the ZDW of 1683 nm, whereas they are chosen to be close to the ZDW of 1826 nm for the fiber fast axis. From Fig. 4, we can see that the flatness of the broadband MI gain profile is gradually improved when the pump wavelength is close to the second ZDWs of the fiber, which illustrates that the amplification bandwidth can be tuned and controlled by changing the pump wavelength in the anomalous dispersion region. Moreover, there exist optimal pump wavelengths along the fiber slow and fast axes. For the fiber slow axis, the optimal pump wavelength is $\lambda_{p,x}^{opt} = 1675$ nm and the corresponding gain bandwidth reaches 110 THz when the pump power is $P_p = 250$ W. For the fiber fast axis, the optimal pump wavelength is $\lambda_{p,y}^{opt} = 1818$ nm and the corresponding gain bandwidth reaches 77 THz when the pump power is $P_p = 600$ W. A further analysis based on Figs. 4(a) and 4(b) reveals that the optimal pump wavelengths (1675 nm and 1818 nm) along the fiber slow and fast axes certainly lie at about 8 nm below their second ZDWs (1683 nm and 1826 nm). The result is consistent with that obtained in the non-birefringent photonic crystal fiber (see Ref. [22]). The above research results show that one can obtain a tunable broadband amplification by using the modulation instability according to the need of the practical applications.

The results discussed above tell us that it is easy to adjust the gain bandwidth by controlling the pump wavelength. But those results are obtained under the conditions of certain pump power, $P_p = 250$ W for the fiber slow axis and $P_p = 600$ W for the fiber fast axis, and they do not reveal whether the broadband tunable gain also depends on the pump power. So the effect of the pump power on the broadband amplification should be studied. Here, with the optimal pump wavelengths obtained above (1675 nm for the fiber slow axis and 1818 nm for the fiber fast axis), the power dependence of the broadband MI gain is shown in Fig. 5. It is worth noting that Figs. 5(a) and 5(c) do not consider the Raman effect while Figs. 5(b) and 5(d) consider it. To better express the MI gain, color is used to represent the normalized MI gain in Fig. 5. Analysing Figs. 5(a)–5(d), we can find that the MI gain profile clearly depends on the pump power, and the gain bandwidth gradually widens with the increase of the pump power. For the fiber slow axis, when $P_p < 175$ W and $\lambda_p = 1675$ nm, a two-peak gain profile appears at the anti-Stokes sideband (see Figs. 5(a) and 5(b)). Similar results also appear along the fiber fast axis (see Figs. 5(c) and 5(d)), and the difference is that the conditions of $P_p < 350$ W and $\lambda_p = 1818$ nm should be satisfied for the fiber fast axis. However, for the fiber slow axis, when $P_p > 175$ W, the two gain peaks merge together, and a single broadband gain profile appears in the anti-Stokes sideband (see Figs. 5(a) and 5(b)). Similar results also appear along the fiber fast axis (see Figs. 5(c) and 5(d)), and the difference is that $P_p > 350$ W and $\lambda_p = 1818$ nm along the fiber fast axis. Moreover, compar-

ing Figs. 5(a) and 5(c) with Figs. 5(b) and 5(d), we can see that the introduction of the Raman effect causes the combination of the gain bandwidths from the Stokes and the anti-Stokes bands, and eventually results in the formation of a broadband amplification. The whole analysis indicates that the MI gain bandwidth can also be tuned by changing the pump power.

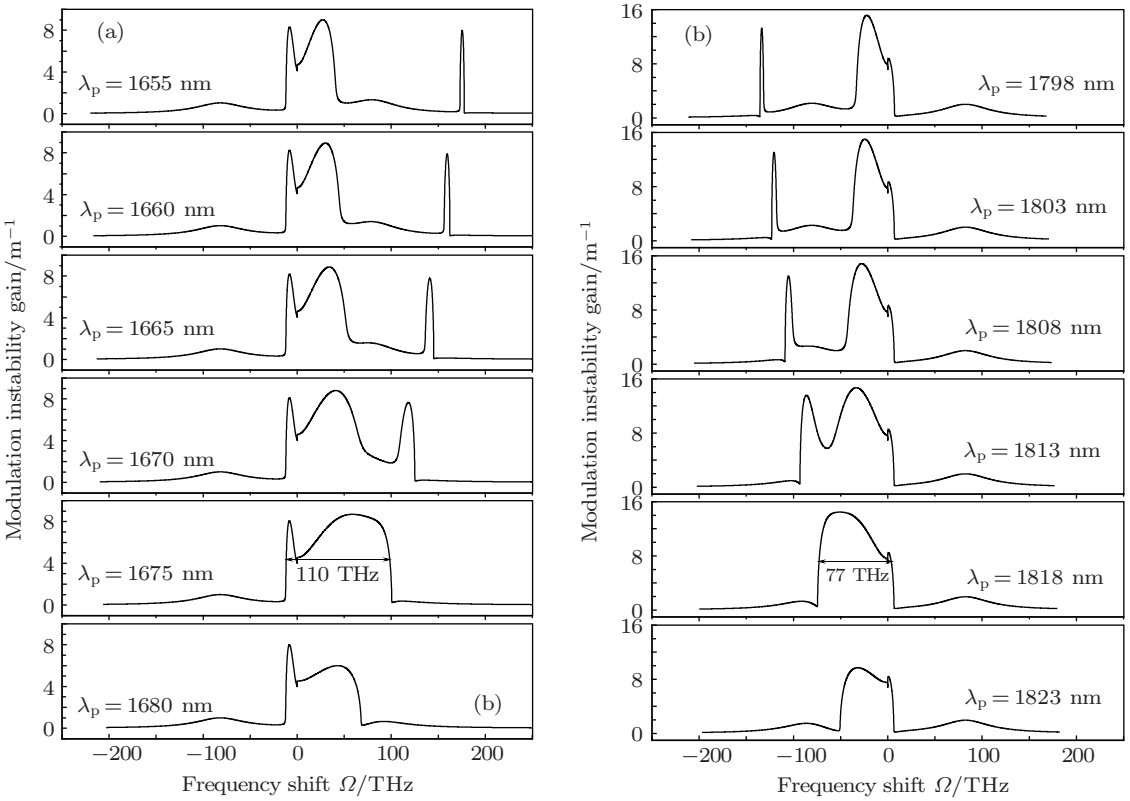


Fig. 4. MI gain variation with the frequency shift: (a) for the fiber slow axis, pump power $P_p = 250$ W, and pump wavelength λ_p is tuned from 1655 nm to 1680 nm; (b) for the fiber fast axis, pump power $P_p = 600$ W, and pump wavelength λ_p varies from 1798 nm to 1823 nm.

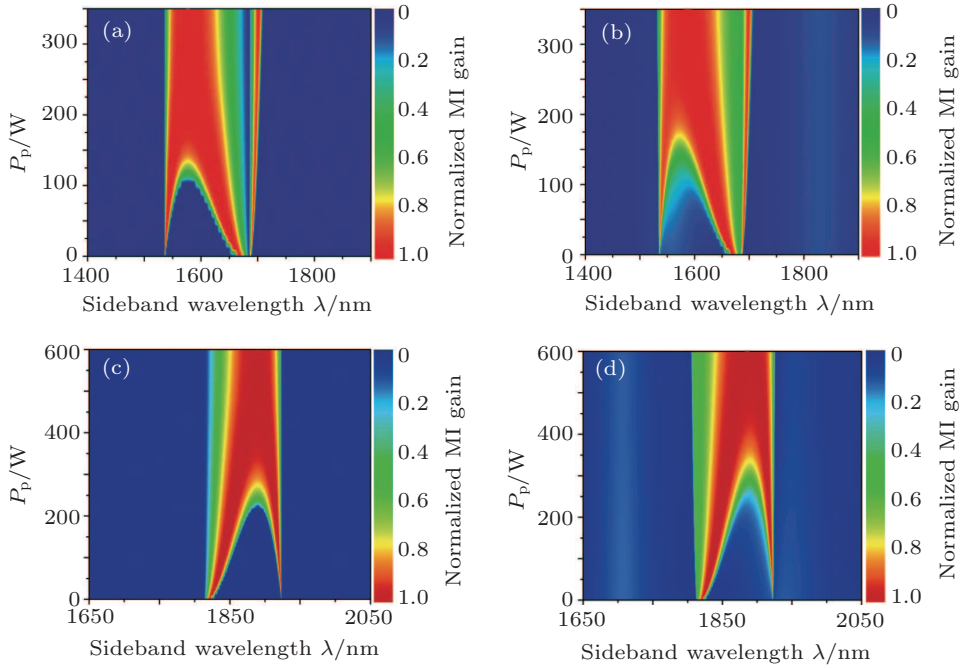


Fig. 5. (color online) Sideband wavelength variation with the pump power: ((a), (b)) for the fiber fast axis, $\lambda_p = 1675$ nm; ((c), (d)) for the fiber slow axis, $\lambda_p = 1818$ nm. In panels (a) and (c), the Raman effect is not considered, while in panels (b) and (d), it is included.

According to the previous findings, an optimal broadband gain can be obtained by choosing an appropriate pump power when the pump wavelengths are $\lambda_{p,x} = 1675$ nm and $\lambda_{p,y} = 1818$ nm. Actually, after the optimal pump wavelengths along the two orthogonal axes of the HB-PCF are determined, the appropriate pump power can first be roughly estimated to be 270 W and 558 W for the two orthogonal axes with the proposed method in Ref. [19], then the optimal pump power can be determined by changing the estimated pump power appropriately. In other words, one may obtain the optimal power by changing the pump power within a certain range around the estimated value. Here, based on the estimated value, the pump power is varied from 250 W to 320 W for the fiber slow axis and from 540 W to 590 W for the fiber fast axis. Figures 6(a) and 6(b) show the broadband MI gain versus the pump power along the two orthogonal axes of the HB-PCF. One can see from Fig. 6 that the optimal pump power is $P_{p,x} = 280$ W for the fiber slow axis, and $P_{p,y} = 570$ W for the fiber fast axis. Moreover, their gain bandwidths finally reach 152 nm and 143 nm, respectively, which are the best numerical results on the MI gain bandwidth so far.

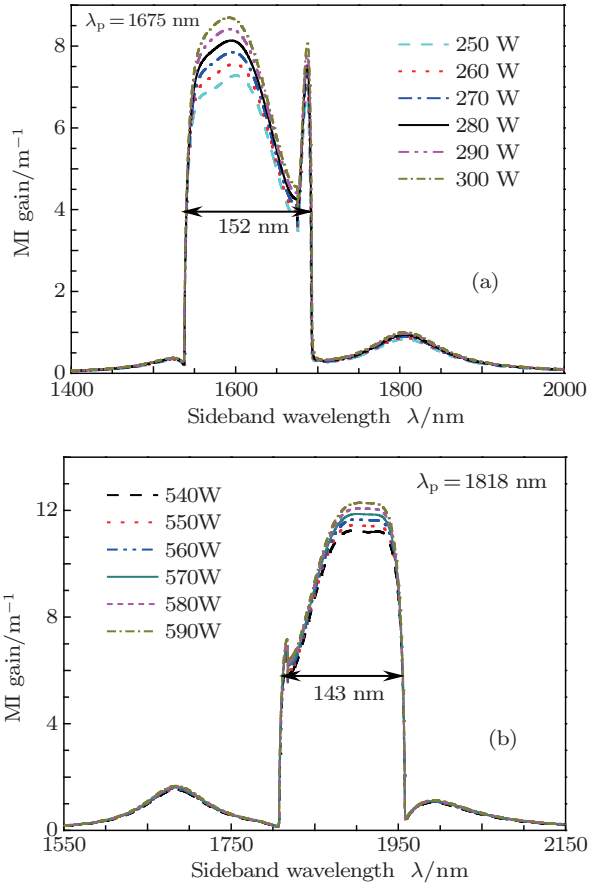


Fig. 6. (color online) Optimal bandwidths of MI gains for different pump powers: (a) at optimal pump wavelength $\lambda_p = 1675$ nm along the fiber slow axis; (b) at optimal pump wavelength $\lambda_p = 1818$ nm along the fiber fast axis.

5. Conclusion

In this paper, a novel HB-PCF with two ZDWs is designed, and an extraordinarily high modal birefringence of 1.56×10^{-2} is obtained at pump wavelength $\lambda_p = 1850$ nm. The two ZDWs along the fiber slow axis are 865 nm and 1683 nm, while along the fiber fast axis, they are 791 nm and 1825 nm. With the designed HB-PCF, the broadband MI gain is comprehensively investigated. The research results show that as long as the pump wavelength lies in the anomalous region of the HB-PCF and is close to their second ZDWs, the amplification bandwidth based on the MI gain characteristic can be tuned by changing the pump wavelength or the pump power due to the combined effect of RS and XPM. Moreover, there exist optimal pump wavelengths and powers along the two orthogonal axes of the HB-PCF, and they are 1675 nm and 280 W for the fiber slow axis, and 1818 nm and 570 W for the fiber fast axis. With the optimal pump parameters, the amplification bandwidths reach 152 nm and 143 nm for the two orthogonal axes of the HB-PCF, respectively, which are the best numerical results on the MI gain bandwidth so far.

References

[1] Xiang A P and Zhong X Q 2010 *Chin. Phys. Lett.* **27** 014203
[2] Wu L and Zhang J F 2007 *Chin. Phys. Lett.* **24** 1471
[3] Wen S C, Su W H and Zhang H 2003 *Chin. Phys. Lett.* **20** 852
[4] Harvey J D, Leonhardt R, Coen S, Wong G K L, Knight J C, Wadsworth W J and Russell P S J 2003 *Opt. Lett.* **28** 2225
[5] Wadsworth W, Joly N, Knight J, Birks T, Biancalana F and Russell P 2004 *Opt. Express* **12** 299
[6] Akheelesh A K, Headley C and Jorgensen C G 2004 *Opt. Lett.* **29** 2163
[7] Tai K, Hasegawa A and Tomita A 1986 *Phys. Rev. Lett.* **56** 135
[8] Wen S C and Fan D Y 2002 *J. Opt. Soc. Am. B* **19** 1653
[9] Agrawal G P 1987 *Phys. Rev. Lett.* **59** 880
[10] Marhic M E, Kagi N, Chiang T K and Kazovsky L G 1996 *Opt. Lett.* **21** 573
[11] Zhang A and Demokan M S 2004 *Opt. Lett.* **30** 2375
[12] Wang Y, Zhang W, Wang Q, Feng X, Liu X M and Peng J D 2004 *Opt. Lett.* **29** 842
[13] Matos C J S, Taylor J R and Hansen K P 2004 *Opt. Lett.* **29** 983
[14] Chen J S Y, Wong G K L, Murdoch S G, Kruhlak R J, Leonhardt R and Harvey J D 2006 *Opt. Lett.* **31** 873
[15] Hilligsöe K M, Andersen T, Paulsen H, Nielsen C, Mölmer K, Keiding S, Kristiansen R, Hansen K and Larsen J 2004 *Opt. Express* **12** 1045
[16] Genty G, Lehtonen M and Ludvigsen H 2004 *Opt. Express* **12** 4614
[17] Ivanov A A, Alfimov M V and Zheltikov A M 2007 *Laser Phys. Lett.* **4** 775
[18] Martins E R, Spadoti D H, Romero M A and Borges B H V 2007 *Opt. Express* **15** 14335
[19] Lin Q and Agrawal G P 2006 *Opt. Lett.* **31** 3086
[20] Dudley J M, Gutty F, Pitois S and Millot G 2001 *IEEE J. Quantum Electron* **37** 587
[21] Zhu Z M and Brown T G 2002 *Opt. Express* **10** 853
[22] Wang H L, Leng Y X and Xu Z Z 2009 *Chin. Phys. B* **18** 5375